Dalton Transactions

Accepted Manuscript

ROYAL SOCIETY OF CHEMISTRY

www.rsc.org/dalton

Structural and Photoluminescence Properties of Stannate based Displaced Pyrochlore-type Red Phosphors: $Ca_{3-x}Sn_3Nb_2O_{14}$: xEu^{3+}

T. S. Sreena, P. Prabhakar Rao*, T. Linda Francis, Athira K. V. Raj and Parvathi S. Babu

Materials Science and Technology Division, CSIR-National Institute for Interdisciplinary Science and Technology (NIIST), Trivandrum – 695 019, India

Abstract

New stannate based displaced pyrochlore-type red phosphors, $Ca_{3-x}Sn_3Nb_2O_{14}$:xEu^{3+} were prepared via conventional solid state method. The influence of partial occupancy of Sn in both A and B sites of the pyrochlore-type oxides on the photoluminescent properties was studied using powder X-ray diffraction, FT-Raman, transmission electron microscope, scanning electron microscope with energy dispersive spectrometer, UV-visible absorption spectroscopy, and photoluminescence excitation and emission spectra with life time measurements. The structural analysis establishes that these oxides belong to a cubic displaced pyrochlore type structure with a space group *Fd-3m.* These phosphors exhibit strong absorptions at near UV and blue wavelength regions and emit intense multiband emissions due to Eu^{3+} $^5D_0$-$^7F_{0,\ 1,\ 2}$ transitions. The absence of characteristic MD transition splitting points out that local cation disorder exists in this type of displaced pyrochlores reducing the D_{3d} inversion symmetry which is not evidenced such disorder in the X-ray diffraction analysis. Unusual forbidden intense sharp $^5D_0$-$^7F_0$ transition indicates single site occupancy of Eu^{3+} with narrower range of bonding environment preventing the cluster formation. This is supported by the stable $^5D_0$ life time with Eu^{3+} concentration. The Judd Ofelt intensity parameters assessment corroborates these results. The CIE color coordinates of these phosphors were found to be (0.60, 0.40) which are close to the NTSC standard values (0.67, 0.33) for a potential red phosphor.

Keywords: Displaced Pyrochlore; Luminescence; Red phosphor

---

* Corresponding author. Tel.: + 91 471 2515311; Fax: + 91 471 2491712

Email ID: padala_rao@yahoo.com (P. PrabhakarRao)

1. Introduction

There is a great demand for inorganic phosphors with high chemical stability and luminescence efficiency for white light emitting diodes that can be effectively excited in the near UV or blue region. In most rare earth or transition metal doped phosphors, light is emitted from only a small number of luminescent centers in the host matrix. The luminescence efficiency of a phosphor material strongly depends on the local coordination structure at the luminescence centers, including factors such as the coordination number, interatomic distance, symmetry and coordinating anion species. Due to the presence of intra-configurational f-f transitions, Eu^{3+} is preferably used as an activator in most inorganic red phosphors. The luminescence of Eu^{3+} ions is determined greatly by the site symmetry and the strength of crystal field at the RE ion site. When Eu^{3+} is located at a low symmetry site, the hypersensitive forced electric dipole $^5D_0 \rightarrow {}^7F_2$ transition dominates over the allowed $^5D_0 \rightarrow {}^7F_1$ transition.[1] In practical inorganic luminescent materials, both electric dipole and magnetic dipole transitions appear simultaneously, although their intensities are different, and in most cases, one of which is much stronger. Therefore, the asymmetric ratio reveals the distortion grade from the inversion symmetry of the local environment in the vicinity of Eu^{3+} in the host matrix. The splitting of these transitions gives an insight into the crystal field effect at the activator sites.[1, 2] The appearance of $^5D_0 \rightarrow {}^7F_0$ transition of Eu^{3+} is an indication of lowering of Eu^{3+} crystal site symmetry as it is allowed only for C_s, C_n, C_{nv} site symmetries and it shows a red shift with the increase in covalency of Eu^{3+}.[3, 4] The failure of Judd- Ofelt theory

in the $^5D_0 \rightarrow {}^7F_0$ transition of Eu^{3+} is due to the mixing of two different states with different J values.[5] The $^5D_0$ and $^7F_0$ levels are non-degenerate and the spectra associated with transitions between them should reflect the crystal-field (CF) splitting of the nominal ^7F_J (or $^{2S+1}L_J$) levels that depend on site symmetry.[6] Further, the site-to-site variation in the local structure around Eu^{3+} will result in the broadening of $^5D_0 \rightarrow {}^7F_0$ transition. Hence Eu^{3+} ions are usually employed as an optical probe to investigate the coordination and environment around the cations substituted in the crystalline lattice.

Pyrochlore oxides (cubic *Fd3m*) with the general formula $A_2B_2O_7$ have attracted extensive attention as host lattice for inorganic phosphors due to its unique properties such as high chemical stability, lattice stiffness, thermal stability, ability to incorporate diverse range of elements at the A and B site and to tolerate both cation and anion disorder etc. The basic framework of the pyrochlore structure is a three dimensional corner sharing MO_6 octahedra, A and B atoms are located on the 16d and 16c positions respectively. The larger A^{3+} cations in eightfold coordination with O^{2-} ions and smaller B^{4+} cations in sixfold coordination with O^{2-} ions are ordered in alternatively <1 1 0> direction.[7] The oxygen has two distinct sites: the oxygen ions on the 48*f* site which are bonded tetrahedrally to two A and B cations and the oxygen ions on the 8*b* sites that are bonded tetrahedrally to four A cations. The A- and B- site coordination polyhedra are joined along edges, and the shape of these polyhedra changes as the positional parameter *x* of O_{48f} shifts to accommodate cations of different sizes. These two polyhedra have D_{3d} symmetry. For $x = 0.3750$ the materials have a defect fluorite structure and $x = 0.3125$, the material have the ideal pyrochlore structure. Thus, the 48*f* oxygen positional parameter *x* defines the polyhedral distortion and structural deviation from the ideal pyrochlore structure.

The occupancy of two types of cation sites in the ideal pyrochlore structure is mainly decided by the ionic radii of the different metal ions at A and B to keep the ratio of the ionic

radius of the cation at A site to that at B site within the tolerance range 1.46-1.80. If the total number of ions at the B site is more than the total number of ions at the A sites, some of the ions occupying the B site might be occupying the A site.[8] This unconventional placement of small B type cations on the large A cation site results in the displacive disorder in the A_2O' network. A number of reports found in the literature suggests that displacive disorder in the A_2O' network is an inherent feature of the pyrochlore structure. Such pyrochlore are termed as misplaced-displacive cubic pyrochlore − pyrochlore which exhibit misplacement of traditionally octahedral B-site cations onto the larger A-sites, accompanied by displacive disorder in the A_2O' substructure to facilitate lower coordination number for the smaller species.[9] Their XRD pattern exhibit weak forbidden reflections (e.g. 442) which serve as a diagnostic flag for the displacement of atoms to lower symmetry positions in the space group and also they show relaxor behavior at low temperature. Detailed studies by Levin *et al.*[10] determined the stoichiometry of single-phase cubic bismuth zinc niobate to be $Bi_{3/2}Zn_{0.92}Nb_{1.5}O_{6.92}$ (BZN) in the pyrochlore structure ($A_2B_2O_6O'$) with partial Zn occupancy of both A and B sites. In addition, displacements from the ideal crystallographic positions were identified for both A and O' ions. The A-site cations were found to be randomly displaced from the ideal eight fold-coordinated positions along the six <1 1 2> directions, perpendicular to the O'-A-O' links. The O' ions were found to be randomly displaced along the <1 1 0> directions. However, to date, only the spectra of BZN have been reported despite the large number of bismuth-based pyrochlore compounds studied in the last decades. The misplaced- displacive cubic pyrochlore have been reported as attractive candidate materials in low-temperature co-fired ceramic (LTCC) multilayer capacitor and integrated device applications, including frequency agile microwave devices and in semiconducting oxides and superconductors.[11-14] Up to now, no details about the photoluminescence work of these configurations have been reported.

Accommodating cations having different valency and ionic radii in the pyrochlore A site can cause change in the luminescent properties. As always, disorder can give the appearance of higher symmetry, the deviation of the pyrochlore A site symmetry from a perfect inversion centre and also the distortion of scalenohedra can improve the luminescence. In this direction, new stannate pyrochlore phosphors $Ca_{3-x}Sn_3Nb_2O_{14}$: xEu^{3+} have been prepared via solid state reaction method in order to investigate the evolution of emission spectra with the partial occupancy of Sn in both A and B sites. The spectra show strong red luminescence through forced electric dipole transition ($^5D_0 \rightarrow {}^7F_2$) under the excitation either into the $^5L_6$ state with 394 nm or the $^5D_2$ state with 465 nm. Interestingly, there is no splitting observed in MD transition $^5D_0 \rightarrow {}^7F_1$ in contrast to the pyrochlore D_{3d} symmetry. Further unusual forbidden intense sharp $^5D_0 \rightarrow {}^7F_0$ transition indicates low symmetry of Eu^{3+} ions with uniform environment or without much site to site variation. The experimental details and the results of these phosphors are presented in this article.

2. Experimental

The pyrochlore type red phosphors with the general formula $Ca_{3-x}Sn_3Nb_2O_{14}$:xEu^{3+} (x = 0.05, 0.10, 0.15 and 0.20) were synthesized by the conventional solid state reaction method using $CaCO_3$, SnO_2, Nb_2O_5, Eu_2O_3 (99.9% purity; Sigma-Aldrich, Steinheim, Germany) as starting materials. The required stoichiometric amounts of these materials were weighed and then thoroughly wet mixed in agate mortar with acetone as the wetting medium. The mixing is followed by drying in an air oven at a temperature of 100°C. This process of mixing and drying was repeated thrice to get a homogeneous product. The obtained mixture was initially calcined at 1300°C for 6h in a platinum crucible in an air atmosphere furnace. The calcination was repeated at 1500°C for 6h with intermittent grinding until a phase pure compound was obtained. The calcined product was then ground into a fine powder for carrying further characterizations.

The crystalline structure and the phase purity of the samples were analyzed by recording the X-ray powder diffraction (XRD) pattern using PANalytical X'Pert Pro diffractometer having Ni filtered Cu–Kα radiation with X-ray tube operating at 40 kV, 30 mA and 2θ varied from 10 to 90º in 0.016 steps. The Raman spectra of the powder samples were acquired using an integrated micro-Raman system using a 633nm helium-neon laser with a spatial resolution of 2µm to analyse the structural aspects of the powder samples. The morphology of powder particles was studied by a scanning electron microscope (Carl Zeiss EVO 18) operated at 20 kV. The X-ray microchemical analysis and elemental mapping of the samples were carried out using Silicon Drift Detector–X-Max^N attached with the SEM. The selected-area electron diffraction (SAED) patterns and high-resolution electron microscopy of the samples were taken using a TECNAI 30G^2 S-TWIN transmission electron microscope (FEI, The Netherlands) operating at 300 kV. Absorbance studies of the samples were carried out using a Shimadzu, UV-3600 UV-Vis spectrophotometer in the 200–500 nm wavelength range using barium sulfate as a reference. The photoluminescence spectra of the prepared samples were obtained using a Spex-Fluorolog DM3000F spectrofluorimeter with a 450 W xenon flash lamp as the exciting source. Luminescence life time of the phosphors was recorded by the phosphorimeter attached to Fluorolog®3 spectrofluorimeter. All the measurements were carried out at room temperature.

3. Results and discussion

3.1. Powder X-ray diffraction studies:

Fig. 1 shows the powder X-ray diffraction patterns of $Ca_{3-x}Sn_3Nb_2O_{14}$:xEu^{3+} (x = 0, 0.05, 0.10, 0.15 and 0.20) phosphors calcined at 1500°C. All the peaks can be well indexed to a cubic pyrochlore structure with a space group *Fd3m* (JCPDS File No: 037-0191). The sharp and intense peaks of the patterns indicate the crystalline nature of the samples. The presence of characteristic super lattice peaks correspond to (111), (311), (511), (531), and (551) lattice

planes evidences the formation of pyrochlore phase. Above 15 mol% doping, minor impurity SnO_2 peaks (marked as *) were observed in the XRD pattern. The ionic radii of Ca^{2+} and Eu^{3+} in eightfold co-ordination are 1.12 and 1.07Å, respectively and that of Sn^{4+} and Nb^{5+} in sixfold co-ordinations are 0.81 and 0.64Å, respectively.[15]As the ionic radius of Ca matches with that of Eu effective doping is possible. The bigger Ca^{2+} and Eu^{3+} ions occupy the A sites and the transition metals Sn^{4+} and Nb^{5+} occupy the B sites. Also since the total number of Sn and Nb ions at the B-sites is more than the total number of Ca and Eu ions at the A-sites, some of the Sn ions might be occupying the A-sites because of its medium ionic radius according to the crystal chemical principle.[16] In this case, the occupation of randomly displacive Sn^{4+} ions makes the system in a disordered state reducing the pyrochlore D_{3d} symmetry as evidenced from the photoluminescence properties. R S Roth et al.[11] had reported that some of the ions in the B-site can be mixed with larger Ca^{2+} ions on the A-sites by displacing it from the ideal 8-coordinated position to achieve satisfactory coordination environment. The structural origin of this behavior is far from clear. From the chemical point of view, extensive displacive disorder is not perhaps unexpected given the presence of rather small Sn^{4+} on the (6+2) fold coordinated pyrochlore A site and the difference in valence of the cations occupying the pyrochlore B site. This behavior has been observed in a number of pyrochlore systems[9] which exhibit static displacive disorder in the A_2O' network that facilitates reduced coordination numbers for the B type cations. The known limits of structural stability for the ideal cubic pyrochlore structure type[7, 10, 15] suggest that it could not be possible for Sn^{4+} to occupy the A site without significant local structural distortion. These results confirm that the present pyrochlore oxides involve mixing of three cations (Ca. Sn and Eu) on the A site and the two types of cations (Sn and Nb) on the B-sites.

The radius ratio (r_A/r_B) is determined by the average ionic radius of the expected elements at the A site (Ca, Sn and Eu) to the B site elements (Sn and Nb). The average ionic radius of the cations occupying the A site and B site is calculated using the formula,

$$r_A = \frac{(3-x)r_{Ca}+xr_{Eu}+r_{Sn}}{4} \quad (1)$$

$$r_B = \frac{2r_{Sn}+2r_{Nb}}{4} \quad (2)$$

The radius ratios of the prepared compounds were calculated accordingly and the values are listed in Table 1. The data show that the ratio decreases with increase in Eu^{3+} ion concentration. The intensity variation of the characteristic super-structure peaks (111) is shown in Fig. 2. The decreasing trend of intensity ratio upto x = 0.10 indicates the probability of Eu^{3+} replacing the Ca (A) site which reduces the radius ratio (r_A/r_B) in turn decreases the order in the lattice. Such variation in the intensities of super structure peaks is associated with the variation in the oxygen position parameter. As the value of 48*f* oxygen positional parameter, x increases A site scalenohedra becomes less distorted, which is evident from decreasing trend of asymmetric ratio with Eu^{3+} ion concentration which is more discussed in the later part. On further substitution, Eu^{3+} is preferring to occupy the Sn displaced (A) site for maintaining the charge neutrality which is further confirmed by the minor SnO_2 secondary phase in the XRD. Further the asymmetric ratio increased due to more distortion of the Eu^{3+} at the Sn site due to mismatch of ionic radius and the displaced environment as discussed below. This led to the intensity ratio increase on higher substitution of Eu^{3+}. It is earlier reported that, as the radius ratio decreases, the pyrochlore structure tends to get converted from a well-ordered structure to disorder structure, in which the super-structure peaks diminish. Reducing the difference in ionic radius between A and B cations in the pyrochlore structure favors disordering. Disorder increases with increasing r_B and decreasing r_A.[17] The lattice parameters of the samples were calculated from the d-spacing. The lattice

parameter increases with increase in Eu^{3+} concentration upto 10 mol%, which is evident from the shift of the (222) peaks towards left and after that it decreases. As Eu^{3+} replaces Ca^{2+} having high ionic radius, lattice value should decrease with increase in Eu^{3+} concentration. Such inconsistency in the XRD pattern may be due to interstitial oxygen ions in the crystal lattice for maintaining the electrical neutrality of the system.

3.2.Raman Spectroscopic Studies:

The crystalline $Ca_{3-x}Sn_3Nb_2O_{14}$:xEu^{3+} (x = 0.05, 0.10, 0.15 and 0.20) samples were examined by Raman spectroscopy to look for further short range structural information, since Raman spectroscopy is an excellent tool to determine the local structure/disorder arising due to the anions in the materials.[18, 19] According to Group theoretical analysis, Raman spectrum of a cubic pyrochlore structure has six optical Raman active modes which are given as:

$$\Gamma_{\text{Raman}} = A_{1g} + E_g + 4F_{2g}$$

These Raman active modes involve only the motion of oxygen atom since A and B cations located at the inversion centre (D_{3d}) do not contribute to Raman active vibrations. One of the F_{2g} modes is caused by the 8*a* oxygen sub-lattice vibration and the other F_{2g} Raman modes are related to 48*f* oxygen sub-lattice vibrations in the cubic pyrochlore lattice.[20, 21] The E_g mode can be assigned to $B\text{-}O_6$ bending vibrations and the A_{1g} mode to O-B-O bending vibrations, while F_{2g} modes represent a mixture of A-O and B-O bond stretching vibrations with bending vibrations.

Fig. 3 represents the Raman spectra of all the samples in the series $Ca_{3-x}Sn_3Nb_2O_{14}$:xEu^{3+} (x = 0.05, 0.10, 0.15 and 0.20) in the wave number ranging from 100 to 1000cm^{-1}. The Raman modes are assigned to symmetry species by referencing the previous literature[18] and the proposed modes assignment is given in Table 2. The Raman modes are

broad as compared to that of well-ordered crystalline compounds, which is due to the inherent disorder in the system. This broadness is not due to small particle size because the sharp and narrow peaks in the XRD diagram and also the SEM analysis had shown that the particle size falls in the micrometer range. Thus the broadening due to small particle size can be ruled out. Moreover, since all the Raman active vibrations involve oxygen motion the origin of broadening is mainly due to structural disorder present in the system due to existence of random vacancy from the statistical nature of the oxygen occupancy among various sites.[17] However, the difference of the cation ion radius in A and B site will affect the force constant of the A-O, A-O', and B-O vibrational modes; thus the whole Raman bands will have some extent of shift to red or blue direction and even some new vibrational modes will emerge.

After analyzing the Raman spectra based on the previously studied pyrochlore spectra, the typical modes of $Ca_3Sn_3Nb_2O_{14}$ were found to be located at 155, 264, 304, 485 and 621cm^{-1}. The appearance of one extra Raman mode at low frequency region (not observed for the ideal pyrochlore structure) in the system indicates the additional displacement of A and O' sites from the ideal atomic positions in the pyrochlore structure. Since the crystalline samples are composite pyrochlores, the A-O bonds include Ca-O and Sn-O bonds while B-O bonds include Nb-O and Sn-O bonds. The mode at 621 cm^{-1} corresponds to the Nb-O stretching modes. Similarly, the modes at 156cm^{-1} and 266 cm^{-1}are related to the Sn-O stretching modes and Ca-O stretching modes of A site, respectively. A new mode at nearly 840cm^{-1} occurs in doped sample which may be due to the vibrational mode originating from localized short-range disorder of B site atoms and subsequent relaxation of the selection rules. In this complex compound, two species ions are located at A and B site which would lead to two different vibrational modes corresponding to low frequency lines (155cm^{-1} and 264 cm^{-1}) both are assigned to F_{2g} mode. The low frequency

vibrations are due to the large cation displacements combined with octahedral deformations which results in a large variation in the A-O bond length chemical environment. Further when the A site (Ca^{2+}) is replaced by a smaller ion like Eu^{3+} in the present case resulting the movement of oxygen atoms closer to the A site cation (along the bisector of the B-O-B angle) thereby decreasing the bond angle and increasing the B-O bond length. The variations of the F_{2g} mode around 155 cm^{-1} and A_{1g} mode around 485 cm^{-1} suggest that excess Sn^{4+} and Eu^{3+} ions are occupying at the A sites.

As suggested from X-ray diffraction results discussed earlier, the Raman observations clearly corroborate the formation of solid solution with Eu^{3+} incorporation in $Ca_{3-x}Sn_3Nb_2O_{14}$:xEu^{3+} (x = 0.05, 0.10, 0.15 and 0.20), since the peaks corresponding to the cubic pyrochlore structure are observed in all the samples. A close look at the peak positions for different Raman modes with Eu^{3+} content, as presented in Table 2, reveals the hardening of F_{2g} (~ 264cm^{-1}) mode with increasing Eu^{3+} concentration. The hardening of F_{2g} mode with increasing Eu^{3+} concentration may be due to the strengthening of A-O bond as a result of Eu^{3+} doping, resulting into bond shortening and thereby shifting this stretching mode toward higher frequencies. On the other hand, the F_{2g} (~ 621cm^{-1}) mode remains more or less same with increasing Eu^{3+} concentration as there is no change in the B site occupation. This indicates that ion concentration in B site does not change but the ion concentration in A site changes with the chemical constitution change. This observation of strengthening of few modes gives a general indication of overall lattice strain and resulting local distortion in the system.[22] Small distortions of the atomic positions caused by B cation species in pyrochlore structure compounds affect the force constant of vibrational mode resulting small shift in vibrational frequency. Thus, the full width at half maximum (FWHM) of a vibrational mode provides a measure of the level of localized short-range structural disorder in the material.[23]

From the structural analysis it can be deduced that Sn^{4+} ions occupy the A site at a displaced position forming displaced pyrochlore phase.

3.3 Morphological studies

Fig. S1 (ES1†) shows the typical SEM micrographs of all the Eu^{3+} -doped samples. The overall morphologies of all the samples are more or less similar. The powder particles appear to be highly crystalline and are slightly agglomerated. The particles are in the scale of 1-5µm in size with homogeneous nature. Elemental X-ray dot mapping analysis of the typical $Ca_{2.85}Sn_3Nb_2O_{14}$:*0.15*Eu^{3+} phosphor calcined at 1500°C for 6h is shown in Fig. 4. This reveals that all the elements are uniformly distributed in the lattice. The chemical composition of the developed phosphors was checked using energy dispersive spectrometry analysis attached with SEM (Fig. S2, ES1†) and identified the presence of all expected elements and the obtained chemical compositions were close to the theoretical stoichiometry. EDS quantification with Eu^{3+} concentration confirms the increase of oxygen content in the lattice indicating the presence of interstitial oxygen.

Fig. 5 shows the typical SAED patterns of (a) $Ca_{2.9}Sn_3Nb_2O_{14}$:*0.1*Eu^{3+} and (b) $Ca_{2.85}Sn_3Nb_2O_{14}$:*0.15*Eu^{3+} phosphors calcined at 1500°C. The SAED pattern shows a polycrystalline nature of the material and the ordered diffraction maxima with weak super lattice diffraction spots (a) further confirms the pyrochlore type unit cell in accordance with the literature[24]. However, due to overlap of the diffraction spots from many crystals such ordered pattern is not seen in the Fig. 5(b).

3.4 Absorbance and Photoluminescent Studies:

The UV-Vis absorption spectra of $Ca_{3-x}Sn_3Nb_2O_{14}$:xEu^{3+} (x = 0.05, 0.10, 0.15 and 0.20) phosphors is given in Fig. 6. All the samples have a broad band of absorption in the UV

region (200-375nm) peaking at around 270nm due to the ligand to metal charge transfer in the stannate/niobate groups and $Eu^{3+} – O^{2-}$ in the host lattice. The degree of absorption of the Eu^{3+} level is increasing with Eu^{3+} concentration upto 15mol%, thereafter it get decreases, indicating that the energy conversion from the CT states to the Eu^{3+} emitting levels is efficiently taking place. The absorption spectra showed a blue shift with increasing concentration of Eu^{3+} and the band gap was calculated from the absorption spectra using Shapiro's method by extrapolating the onset of absorption to the wavelength axis and the estimated band gap energies are tabulated in Table 3. Thus it is expected that the phosphors can be effectively excited under both UV and visible region, which is further confirmed from the excitation spectra and it is one of the prerequisites for a phosphor material for pc WLEDs.

The influence of the partial substitution of Sn in both A and B sites of the pyrochlore-type oxides on the photoluminescent properties were investigated by recording the PL spectra of the developed phosphors at room temperature under identical instrumental conditions. The excitation spectra were measured by monitoring the peak intensity at 613nm. Fig. 7 shows the excitation spectra of $Ca_{3-x}Sn_3Nb_2O_{14}:xEu^{3+}$ (x = 0.05, 0.10, 0.15, and 0.20) which include a broad charge transfer (CT) band from 250-360nm centered at 306nm followed by a series of sharp peaks beyond 360nm. The broad CT band is due to the merged effect of $O_{2p} \rightarrow Eu_{4f}$ and $O_{2p} \rightarrow Nb_{4d}$ charge transfer transitions. This broad band is mainly attributed to the charge transfer excitation of Eu^{3+} and the energy transfer transition from tin and niobium groups to the Eu^{3+} ions.[25] In complex hosts, the contributions from more than one component in the CT band cannot be resolved due to spectral overlap.[4,26] The CT band is red shifted with Eu^{3+} doping concentration. This shift can be attributed to an increase in covalency of Eu–O bond and the coordination environment of Eu^{3+} environment, which reduces the CT energy. The sharp peaks beyond 360nm are due to the intra-configurational (f-f) transitions of Eu^{3+} including the peaks with maxima at 362nm ($^7F_0$-$^5D_4$), 382nm ($^7F_0$-$^5G_{2-4}$), 394nm ($^7F_0$-$^5L_6$),

412nm ($^7F_0$-$^5D_3$) and 464nm ($^7F_0$-$^5D_2$).[27] The f-f transition peaks are less intense compared to the broad charge transfer band and are saturated for 15mol% doping. Among them, the intensity of the peaks at 394nm and 464nm excitation wavelengths which are emission lines of near UV and blue LED chips is much stronger than the other transitions from Eu^{3+}. This implies that these samples can be effectively excited by radiations of wavelength in the near UV and blue regions.

Fig. 8 shows the emission spectra of $Ca_{3-x}Sn_3Nb_2O_{14}$:$x$$Eu^{3+}$ (x = 0.05, 0.10, 0.15, and 0.20) phosphors excited at 394nm. The major emission peaks are observed at 575, 586, 614, 630 and 660nm which can be assigned to $^5D_0$ -^7F_J (J = 0, 1, 2, 3, 4) transitions of Eu^{3+} ion. According to J–O theory, [31, 32] the emission lines are a cumulative effect of the magnetic dipole (MD) transition and the electric dipole (ED) transition depending on the specific environment of Eu^{3+}. When the Eu^{3+} ions embedded in a site with inversion symmetry, the $^5D_0$ -$^7F_1$ magnetic dipole transition is dominating, while in a site without inversion symmetry the $^5D_0$ -$^7F_2$ electric dipole transition is the strongest. In the present system, the red emission peak at 614 nm is more dominant which is due to the $^5D_0$-$^7F_2$ ED transition of Eu^{3+} which indicates that Eu^{3+} occupies a non-centrosymmetric site.[28] The sharp emission without splitting at 586nm i.e., orange region is assigned to MD transition ($^5D_0$-$^7F_1$) and it is insensitive to the site symmetry. When RE ion locates in a site without inversion symmetry, the odd 4f-orbitals mix with either even 5d orbital or charge transfer orbital so that the parity selection rule is relaxed. For Eu^{3+} ions, the energy of the 5d orbital is higher than CT band, so the mixing of CT band with the f- orbital mainly contributes for the enhancement of forced ED transitions.[28] Based on the D_{3d} symmetry at A site, the MD transition is expected to have splitting into two as observed in the normal pyrochlore.[26,29] In contrast to this, no such splitting is observed in the present displaced pyrochlore system. As discussed in the earlier literature[30, 9-11,] displaced pyrochlores exhibit substantial displacive disorder in the

A_2O'subnetwork. Dielectric relaxation is reported as the characteristic of the displacive disorder. Here, the luminescence results suggest that the single sharp emission due to MD transition is a characteristic of such displacive disorder pyrochlore due to loss of D_{3d} inversion symmetry.

One important observation is that $^5D_0$-$^7F_0$ transition is more intense than $^5D_0$-$^7F_1$ transition. It has been confirmed that $^5D_0$-$^7F_0$ is highly forbidden for both electric dipole and magnetic dipole transition in a Eu^{3+} doped compound,[31-33] therefore this abnormal phenomenon is not in agreement with Judd-Ofelt theory. Also the $^7F_0$ and $^5D_0$ levels are non-degenerate and the spectra associated with transitions between them should contain as many lines as the number of host non-equivalent sites.[34] The splitting in this transition points out the dual or more non-equivalent site occupancy of Eu^{3+} ions.[35] But, in our system $^5D_0$-$^7F_0$ levels exhibits sharp and single peak which offers the possibility of doping of Eu^{3+} ion to the Ca site. The unusually strong $^5D_0$-$^7F_0$ transitions have been reported in other materials, [5, 36-42] there are different explanation for this phenomenon. One explanation is based on the mixing of two different states with different *J* values, the breakdown of Wybourne-Downer mechanism and relativistic effects.[41-43] Secondly, the appearance of $^5D_0 \rightarrow {}^7F_0$ transition of Eu^{3+} is an indication of lowering of Eu^{3+} crystal site symmetry as it is allowed only for C_s, C_n, C_{nv} site symmetries.[3,4,44] Thirdly, the microstructure can also induce this transition.[39]It has been reported that, the extra oxygen in the lattice is responsible for the unusually strongest $^5D_0 \rightarrow {}^7F_0$ transitions in Eu^{3+} doped Y_3SbO_7.[45] In our system, last explanation is suitable because the lattice parameter calculated from the peak position in the XRD pattern confirms the presence of interstitial oxygen in the crystal lattice. The observation of this peak in the emission spectra indicates that forbidden $^5D_0$-$^7F_0$ transition can be relaxed by distortion of Eu^{3+} environment. However, in the present system, the red emission intensity is more compared to any other transitions and it increased with increase in doping concentration. The

enhanced ED transition intensity arises from the symmetry distortion of Eu^{3+} in most cases. Incorporation of cations with different valency and electronegativity to the crystal lattice was the reason for distortion of A site of present pyrochlore system. The distortion of the A site symmetry and the red shift of the charge transfer energy leads to intense $^5D_0$-$^7F_2$ hypersensitive ED transition under 394nm excitation. The emission lines are similar for excitation wavelengths 394 and 464nm. However it is observed that the red emission intensity excited at near UV region (394nm) is greater than that of the emission excited at blue region 464nm.

The asymmetric ratio (intensity of $^5D_0$-$^7F_2$/intensity of $^5D_0$-$^7F_1$) is a good measure of degree of distortion of the scalenohedron and the phase purity of the red color. The asymmetric ratio reveals the distortion grade from the inversion symmetry of the local environment in the vicinity of Eu^{3+} in the host matrix. For $Ca_{3-x}Sn_3Nb_2O_{14}$:$x$$Eu^{3+}$ (x = 0.05, 0.1, 0.15, and 0.2) phosphors, the asymmetric ratio decreases upto 15mol% Eu^{3+} concentrations and then increases and the results are shown in the Table 3. The doping of Eu^{3+} ions to Ca^{2+} sites will decrease the amount of divalent ions in the crystal lattice, which can cause an increase in lattice symmetry and as result the asymmetric ratio decreases. It can also be noted that the full width half maximum (FWHM) of the red peak increases with increase in Eu^{3+} doping concentration upto x = 0.15 and then decreases. This observation can be attributed to concentration quenching.[46, 47] In summary, the emission spectra of the present stannate based displaced pyrochlore-type red phosphors: $Ca_{3-x}Sn_3Nb_2O_{14}$: $x$$Eu^{3+}$, exhibits the allowed magnetic dipole transition, $^5D_0$-$^7F_1$ along with the forced electric dipole transition, $^5D_0$-$^7F_2$ and the forbidden transition, $^5D_0$-$^7F_0$ which are contrary to the D*3d* symmetry of the pyrochlore structure. The presence of these transitions are mainly attributed to the distortion of symmetry of Eu^{3+} environment, mixing of $^5D_0$ states with the charge transfer states and the

presence of interstitial oxygen in the lattice. Further, the splitting of $^5D_0$-$^7F_1$ transition is not observed as attributed to the displaced disorder in the lattice.

The photoluminescence decay curve for $^5D_0$-$^7F_2$ transition of the prepared phosphors under 394nm excitation $Ca_{3-x}Sn_3Nb_2O_{14}$:xEu^{3+} (x= 0.05, 0.1, 0.15, and 0.2) is shown in Fig. 9. All the decay curves can be fitted well using the single exponential decay function,

$$I = A\exp(-t/\tau) \qquad (3)$$

where I, τ and A are intensity, decay time and fitting parameter respectively.

On the basis of the emission spectra and lifetimes of the $^5D_0$ emitting level, the emission quantum efficiency (η) of the Eu^{3+} ion excited state can be determined[48-50] and the calculation procedure is given in ES1†. The life time values and the calculated quantum efficiencies of the phosphors were listed in Table 4. The lifetime of the $^5D_0$ excited state is mainly a result of the radiative and non-radiative decay rates. Here it is observed that the luminescence decay time of red emission (613 nm) of $Ca_{3-x}Sn_3Nb_2O_{14}$:xEu^{3+} (x = 0.05, 0.1, 0.15, and 0.2) remains almost constant (1.26 – 1.28 ms) though concentration quenching is observed beyond 15mol% Eu^{3+}. To some extent here the concentration quenching is observed due to the secondary phase formation as evidenced from the XRD. As discussed above Eu^{3+} ion probably prefers to replace Sn instead of Ca at the A site of pyrochlore for maintaining the charge neutrality for higher substitution leading to minor SnO_2 secondary phase. However, the life time remains the same due to Eu^{3+} at more distorted environment in a displaced position of the A site of the pyrochlore. The decay life times (τ) are proportional to the transition probability. A heavier distortion of the crystallographic sites usually denotes the higher transition probability of Eu^{3+} ions. Thus the higher lifetime of the sample further confirms the more uniform distribution of Eu^{3+} ions in the $Ca_3Sn_3Nb_2O_{14}$ lattice.[51] These long life times could cause the emission to saturate when excited with high light intensities of

commercial LEDs and attain the saturation only at much higher intensities, due to the low absorption cross section of Eu^{3+}. The quantum efficiency calculated from the life time values were in the range of 27-30% with increasing Eu^{3+} concentration.

The J-O intensity parameters Ω_t (2, 4 and 6) of the Eu^{3+} in the matrix $Ca_{3-x}Sn_3Nb_2O_{14}$:xEu^{3+} (x = 0.05, 0.1, 0.15 and 0.2) were calculated to reveal the information regarding the covalence and surrounding of the metal ion. These intensity parameters provide the information regarding the luminescence site symmetry, luminescence behavior and radiative probabilities of activator ion in different host lattices. The parameter Ω_2 determines the covalency, polarizability and the asymmetric behavior of the activator and the ligand (short range effects) whereas Ω_4 are related to long range effects. The J-O intensity parameters $\Omega_{2\text{-}4}$ and other spectral parameters such as branching ratio (β), stimulated cross section (σ) were calculated as described previously[52-55] and the procedure for calculation is given in the ES1†. The Judd-Ofelt intensity parameters and the spectral parameters are listed in Table 4. Since Ω_2 is most sensitive to the ligand environment, its value could reflect the asymmetry of the local environment at the Eu^{3+} ion site. The value of Ω_2 remains almost constant with Eu^{3+} concentration (upto 15mol %) and then increases indicating the increasing asymmetric nature of Eu^{3+} in the host. Generally, the order of the intensity parameters Ω_t is $\Omega_2<\Omega_4$, but in our system the trend is reversed $\Omega_2>\Omega_4$. This change in trend is also in agreement with those reported previously.[52, 53] It means that the efficiency for the $^5D_0$-$^7F_2$ transition becomes weak at the cost of the $^5D_0$-$^7F_1$ transition. The emission intensity could also be characterized by Ω_4 parameters. The continuous increase in the Ω_4 parameter with Eu^{3+} concentration suggests the increased efficiency of $^5D_0$-$^7F_2$ transition which is also evidenced in Table 4. This is further supported by the increase in branching ratio of the $^5D_0$-$^7F_2$ transition compared with other transitions. The calculated value of radiative life time

provided in the Table 4 indicate that this phosphor can be an effective luminescent material. The emission cross section (σ) changes differently for all the three transitions.

The CIE color coordinates of all four samples were calculated to be (0.60, 0.40) using the software CIE Calculator which is close to the NTSC standard values (0.67, 0.33) for a potential red phosphors. Thus, the developed red phosphors could be a suitable candidate for the red components in pc-WLEDs.

4. Conclusions

A series of stannate based displaced pyrochlore type red emitting phosphors $Ca_{3-x}Sn_3Nb_2O_{14}$:xEu^{3+} (x = 0.05, 0.1, 0.15 and 0.2) were prepared by the conventional solid state reaction method for the first time. The influence of the partial substitution of Sn in both A and B sites of the pyrochlore-type oxides on the photoluminescent properties was studied in detail. Our results demonstrate that displacive disorder is not well evidenced by powder X-ray diffraction studies whereas Raman spectral studies indicate some amount of disorder in the lattice. Conversely photoluminescent studies exhibit intense multiband emissions due to Eu^{3+} $^5D_0$-$^7F_{0,\,1,\,2}$ transitions. The absence of characteristic MD transition splitting confirms the local cation disorder in this type of displaced pyrochlores. This can also be considered to be a characteristic of displaced pyrochlores in addition to the dielectric relaxation as reported in the literature.

Acknowledgements:

One of the authors, Sreena T S would like to acknowledge Department of Science and Technology (DST) INSPIRE programme, Council of Scientific and Industrial Research (CSIR), Govt. of India for the research facilities and financial support. The authors thank

Mrs. S G Jiji from the Department of Optoelectronics, University of Kerala for Raman analysis.

References

1 G.Blasse and B. C.Grabmair, *Luminescent Materials*, Springer, Berlin, 1994.

2 J. A. Capobianco, P. P. Proulx, M. Bettinelli and F. Negrisolo, *Phys. Review B,* 1990, 42, 5936−5944.

3 F.Du, R.Zhu, Y.Huang, Y.Tao and H.Jin Seo, *Dalton Trans*., 2011, 40, 11433−11440.

4 Y.Su, L. Li and G. Li, *Chem. Mater.*, 2008, 20, 6060-6067.

5 A. K. Parchur and R. S. Ningthoujam, *RSC Advances*, 2012, 2, 10859-10868.

6 X. Y. Chen, W. Zhao, R. E. Cook, and G. K. Liu, *Phys Review B*, 2004, 70, 205122-205130

7 M. A. Subramanian, G. Aravamudan and G. V Subba Rao, *Prog. Solid State Chem.,* 1983, 15, 55-143.

8 M. Deepa, P. Prabhakar Rao, A.N. Radhakrishnan, K.S. Sibi, and Peter Koshy, *Material Research Bulletin*, 2009, 44, 1481-1488.

9 T. A. Vanderah, I. Levin and M. W. Lufaso, *Eur. J. of Inorg. Chem.*, 2005, 14, 2895-2901.

10 I. Levin, T. G. Amos, J. C. Nino, T. A. Vanderah, C. A. Randall, and M. T. Lanagan, *J. Solid State Chem.* 2002, 168, 69-75.

11 R.S. Roth, T. A. Vanderah, P. Bordet, I. E Grey, W. G. Mumme, L. Cai and J. C. Nino, *J. of Solid State Chem.*, 2008, 181, 406-414.

12 C.A. Randall, J.C. Nino, A. Baker, H. J.Youn, A. Hitomi, R.Thayer, L.F. Edge, T. Sogabe, D. Anderson, T.R. Shrout, S. Trolier-McKinstry and M.T. Lanagan, *Amer. Ceram. Soc. Bull.*, 2003, 82, 9101-9108.

13 W. Ren, S. Trolier-McKinstry, C.A. Randall, and T.R. Shrout, *J. Appl. Phys*., 2001, 89, 767-774.

14 Young. P. Hong, Seok Ha, Ha Yong Lee, Young Cheol Lee, Kyung Hyun Ko, Dong-Wan Kim, Hee Bum Hong and Kug Sun Hong, *Thin Solid Films,* 2002, 419 , 183-188.

15 R D Shannon, *Acta Crystallogr*., 1976, A. 32, 751-767.

16 Wang Hong, Du Huiling and Yao Xi, *Materials Science and Engineering*, 2003, B99, 20-24.

17 Licia Minervini and Robin W. Grimes, *J. Am. Ceram. Soc.*, 2000, 83, 1873-78.

18 M.T. Vandenborre, E Husson, J.P. Chatry and D Michel, *J. Raman Spectroscopy*, 1983, 14, 63-71.

19 B.P. Mandal, Ankita Banerji, Vasant Sathe, S.K. Deb, A.K. Tyagi, *Journal of Solid State Chem.*, 2007, 180 , 2643–2648.

20 H.C. Gupta, P. Ashdhir, C. C.S. Rawat, *J. Phys. Chem. Solids*, 1996, 57, 1857-1859.

21 B. D.Begg, N. J. Hess, D. E. McCready, S. Thevuthasan and W. J. Weber, *J. Nuclear Mater.* 2001, 289,188-193

22 Chunlei Wan, Zhixue Qu, Aibing Du and Wei Pan, *Acta Mater.* 2009, 57, 4782-4789.

23 B.P. Mandal, N. Garg, S.M. Sharma and A.K. Tyagi, *J. Solid State Chem.*, 2006, 179, 1990–1994.

24 Linggen Kong, Inna Karatchevtseva, Mark G Blackford, Nicholas Scales and Gerry Triani, *J. Am. Ceram. Soc.* , 2013, 96, 2994-3000.

25. P. S. Dutta and A. Khanna, *ECS J of Solid State Science and Technology*, 2013, 2, R3153-R3167.

26 S. K. Mahesh, P. Prabhakar Rao, Mariyam Thomas, T. Linda Francis and Peter Koshy, *Inorganic Chemistry*, 2013, 52, 13304–13313.

27 M. Thomas, P. Prabhakar Rao, V. R. Reshmi, T. Linda Francis and Peter Koshy, *J. Am. Ceramic. Soc.*, 2012, 95, 2260-2265.

28 G. Blasse, Chemistry and physics of R-activated phosphors, in: K.A. Gschneider Jr, L.Eyring (Eds.), Handbook on the Physics and Chemistry of Rare-Earths, North-Holland, Amsterdam, 1979.

29 Z. Lu, J. Wang, Y. Tang and Y. Li, *J. Solid State Chemistry*, 2004, 177, 3075-3079.

30 Yun Liu, Ray L. Withers, Hai Binh Nguyen , Kim Elliott , Qijun Ren and Zhanghai Chen, *J. Solid State Chemistry*, 2009, 182, 2748-2755.

31 B. G. Wybourne; *J. Alloys and Compd*, 2004, 380, 96-100.

32 B.R. Judd, *Phys. Rev.*, 1962, 127, 750-761.

33 G.S. Ofelt, *J. Chem. Phys.*, 1962, 37, 511-520.

34 F.Du, R. Zhu, Y. L. Huang, Y. Tao and H. J. Seo, *Dalton Trans.* , 2011, 40, 11433-11440.

35 K. Binnemans and C Gorller Walrand, *J. of Rare Earths*, 1996, 14, 173-180.

36 L Smentek and A. Kędziorski, *J. Alloys Compd*., 2009, 488, 586-590.

37. A. S. Souza, Y. A. R. Oliveira and M. A. Couto dos Santos, *Opt. Mater.*, 2013, 35, 1633-1635.

38 A. M. Pires, M. R. Davolos and O. L. Malta, *J. Lumin.*, 1997, 72, 244-246.

39 B. Piriou, M. Richard-Plouet, J. Parmentier, F. Ferey andS. Vilminot, *J. Alloys and Compd.*, 1997, 262, 450-453.

40 N. Lakshminarasimhan and U. V. Varadaraju, *J. Solid State Chem.*, 2004, 177, 3536-3544.

41 F. Fujishiro, R. Sekimoto and T. Hashimoto, *J. Lumin.*, 2013, 133, 217-221.

42 F. Fujishiro, M. Murakami, T. Hashimoto and M. Takahashi, *J. Ceram. Soc.*, 2010, 118, 1217-1220.

43 M. C. Downer, G. W. Burdick and D. K. Sardar, *J. Chem. Phys.*,1988, 89, 1787-1797.

44 N. J. Cockroft, S. H. Lee and J. C. Wright, *Phys. Rev. B*, 1991, 44, 4117-4126.

45 Jing Wang, Yu Cheng, Yanlin Huang, Peiqing Cai, Sun Il Kim and Hyo Jin Seo, *J. Mater. Chem. C*, 2014, 2, 5559-5569.

46 G Blasse, *Phys. Lett A*, 1968, 28, 444-445.

47 Enhai S, Weiren Z, Guoxiong Z, Xihua D, Chunyu Y, and Minkang Z, *J of Rare Earths*, 2011, 29, 440–443.

48 Y. Su, L. Li, G. Li, *Chem. of Mater.* 2008, 20, 6060-6067.

49 C. Peng, H. Zhang, J. Yu, Q. Meng, L. Fu, H. Li, L. Sun, X. Guo, *J. Phys. Chem. B* 109, 2005, 15278-15287.

50 T. Linda Francis, P. Prabhakar Rao, Mariyam Thomas, S. K Mahesh, V. R. Reshmi, J *Mater Sci. Mater Electron*, 2014, 25, 2387-2393.

51 William M. Yen, Shigeo Shionoya and H. Yamamoto, (Phosphor Handbook, 2006).

52 Athira K V Raj, P Prabhakar Rao, T S Sreena, S Sameera, Vineetha James and U A Renju, *Phy. Chem. Chem.Phy.* , 2014, 16, 23699-23710.

53 Vinod Kumar, Vijay Kumar, S Som, M Duvenhage, O M Ntwaeaborwa, H C Swart, *Appl. Surf Sci.*, 2014, 308, 419-430

54 S. Som, P. Mitra, Vijay Kumar, Vinod Kumar, J. J. Terblans, H. C. Swarta andS. K. Sharma, *Dalton Trans.*, 2014, 43, 9860- 9871.

55 Santosh K. Gupta, M. Mohapatra, S. V. Godbole and V. Natarajan, *RSC Adv.*, 2013, 3, 20046-20053.

Table 1: Variation in lattice parameter, average crystallite size and radius ratio of $Ca_{3-x}Sn_3Nb_2O_{14}$:xEu^{3+} (x = 0.05, 0.10, 0.15 and 0.20) red phosphors.

x	Lattice Parameter(Å)	Average Crystallite size, Δd(μm)	Radius Ratio, r_A/r_B
0	10.401	0.139	1.568
0.05	10.416	0.139	1.567
0.10	10.426	0.106	1.566
0.15	10.423	0.139	1.565
0.20	10.422	0.166	1.564

Table 2: Raman mode frequencies with symmetry character and modes of vibration of $Ca_{3-x}Sn_3Nb_2O_{14}$:xEu^{3+} (x = 0.05, 0.10, 0.15 and 0.20) red phosphors.

Wavenumber (cm^{-1})					Symmetry	Mode of vibration
x=0	x=0.05	x=0.10	x=0.15	x=0.20		
155	155	154	154	153	F_{2g}	A-O stretching
264	266	269	270	272	F_{2g}	A-O stretching
304	306	304	305	303	E_g	O-B-O bond bending
485	487	488	490	493	A_{1g}	O–B–O bending with mixture of B–O stretching
621	620	620	619	619	F_{2g}	B–O stretching
840	840	838	835	834	A_{1g}	B–O stretching

Table 3: Asymmetric ratio and FWHM of the $^5D_0$-$^7F_2$ transition under 394nm excitation and the band gap energy of the as-prepared $Ca_{3-x}Sn_3Nb_2O_{14}$:xEu^{3+} (x = 0.05, 0.10, 0.15 and 0.20) phosphors

x	Asymmetric Ratio	FWHM (nm)	Band gap energy, E_g (eV)
0.05	1.94	7.90	3.60
0.10	1.82	11.72	3.64
0.15	1.69	13.70	3.86
0.20	1.84	10.51	3.89

Table.4. Spectral parameters, life time and quantum efficiency of $Ca_{3-x}Sn_3Nb_2O_{14}:xEu^3$($x$ = 0.05, 0.10, 0.15 and 0.20) phosphors

x	J-O Intensity parameters Ω_2 (pm^2)	Ω_4 (pm^2)	Transitions	$A_{0-2,4}$ (s^{-1})	A_τ (s^{-1})	τ_{rad} (ms)	β (%)	σ (λ_p)	τ (ms)	η (%)
0.05	2.86	1.50	$^5D_0$-$^7F_1$	___	217.71	4.59	22.97	132.93	1.26	27.43
			$^5D_0$-$^7F_2$	157.68			72.43	109.59		
			$^5D_0$-$^7F_4$	3.95			1.81	496.94		
0.10	2.88	1.52	$^5D_0$-$^7F_1$	___	218.39	4.58	22.89	141.81	1.27	27.74
			$^5D_0$-$^7F_2$	159.26			72.92	106.95		
			$^5D_0$-$^7F_4$	4.01			1.84	489.27		
0.15	2.85	1.52	$^5D_0$-$^7F_1$	___	216.92	4.61	23.05	148.48	1.28	27.77
			$^5D_0$-$^7F_2$	157.63			72.67	104.84		
			$^5D_0$-$^7F_4$	3.99			1.84	491.99		
0.20	3.24	1.55	$^5D_0$-$^7F_1$	___	238.50	4.19	20.96	183.95	1.27	30.29
			$^5D_0$-$^7F_2$	178.78			74.96	125.48		
			$^5D_0$-$^7F_4$	4.09			1.71	592.69		

Fig. 1

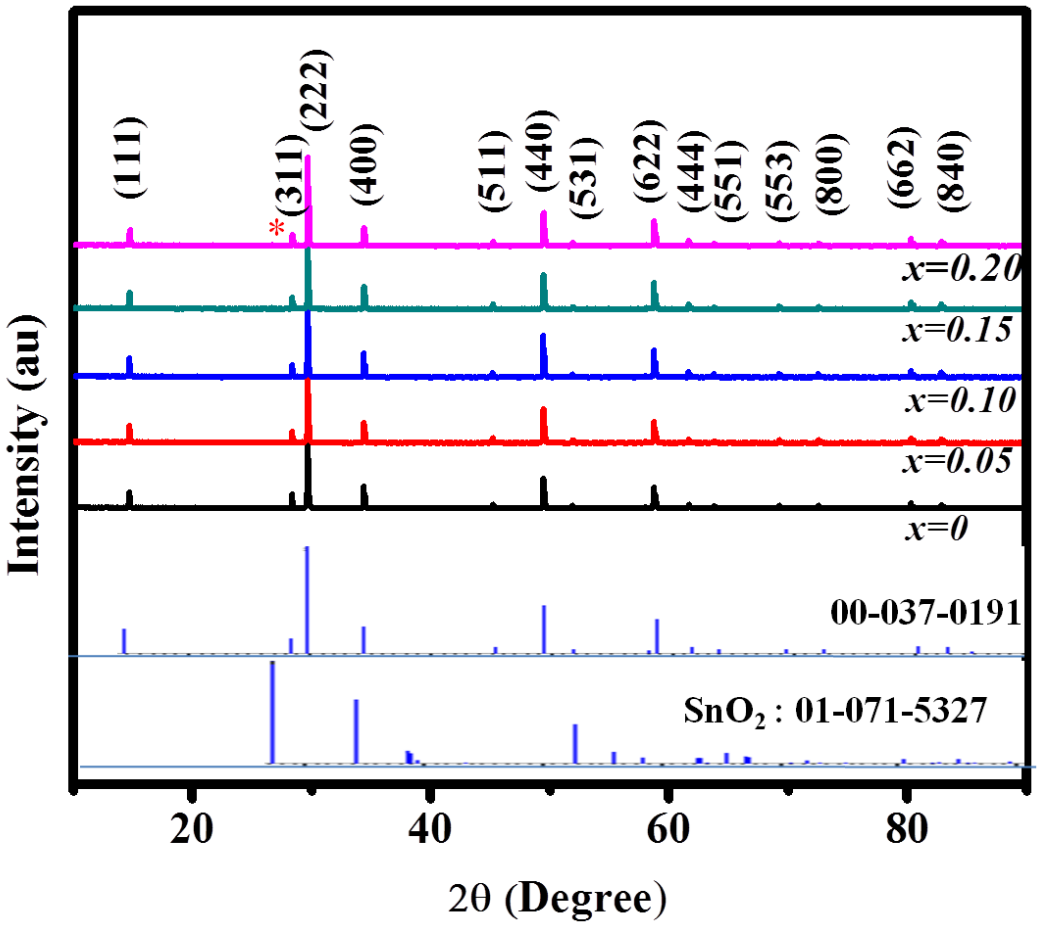

Fig. 1 Powder X-ray diffraction patterns of $Ca_{3-x}Sn_3Nb_2O_{14}$:xEu^{3+} (x = 0, 0.05, 0.10, 0.15 and 0.20) red phosphors synthesized at 1500°C and the reference patterns for pyrochlore and SnO_2. The XRD patterns can be indexed to cubic pyrochlore structure with space group *Fd3m*. Minor impurity SnO_2 peaks (marked as *) were observed above 15 mol% doping.

Fig. 2

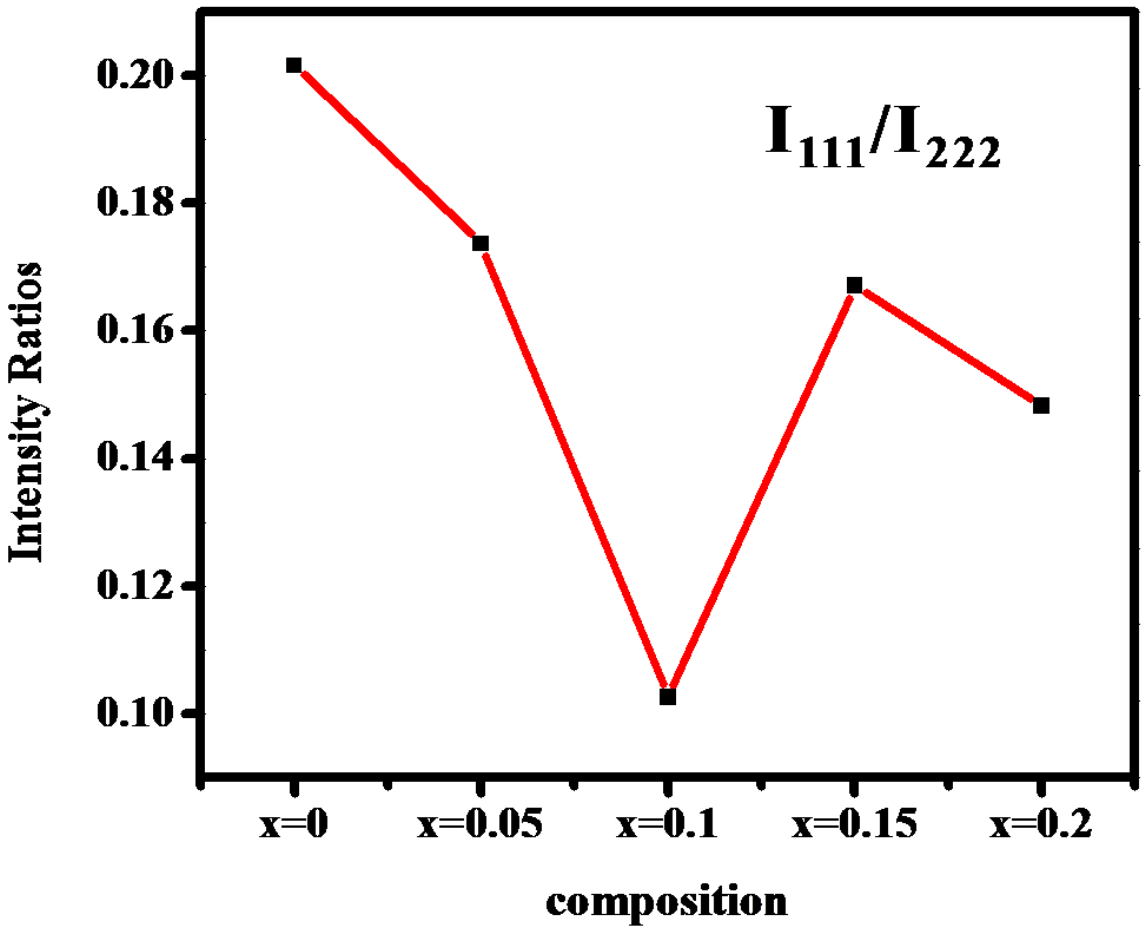

Fig. 2 Variations of super lattice peak intensity ratio I_{111}/I_{222} as a funcion of the composition. The super structrure peaks diminishes with Eu^{3+}concentration.

Fig. 3

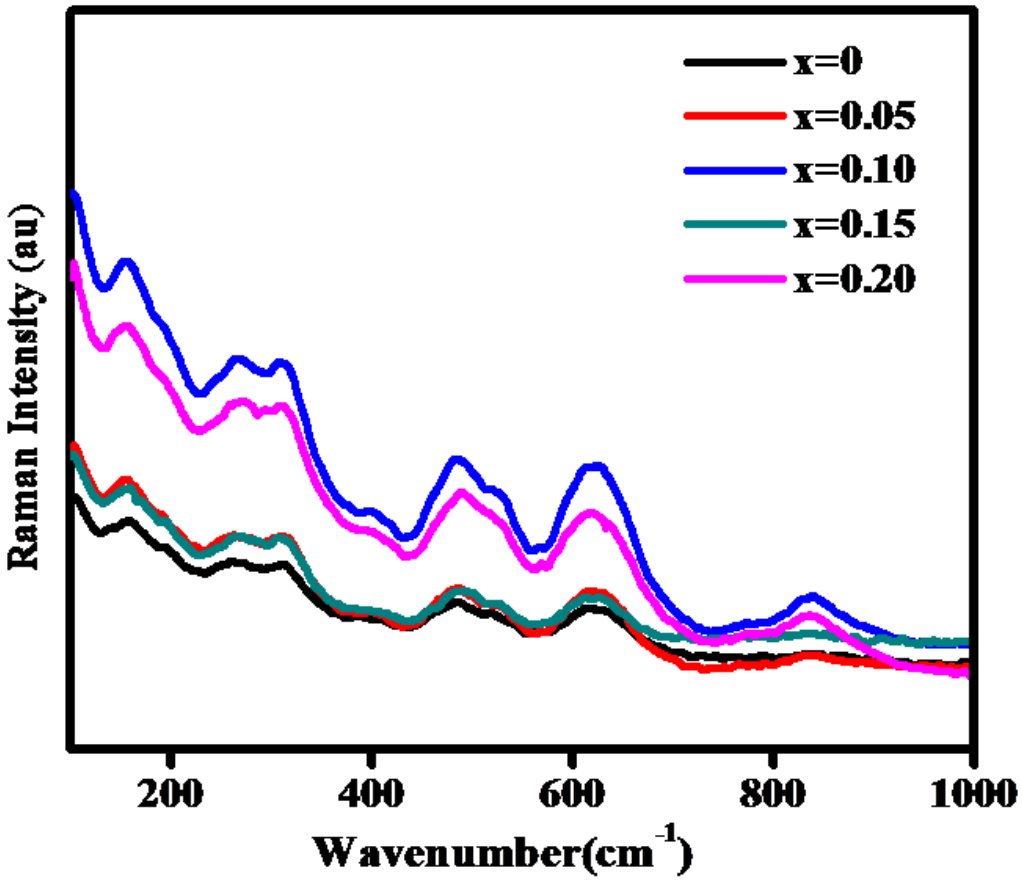

Fig. 3 FT Raman spectra of $Ca_{3-x}Sn_3Nb_2O_{14}$:xEu^{3+} (x = 0.05, 0.10, 0.15 and 0.20) phosphors. All the peaks were corresponds to characteristic pyrochlore peaks. The mode appearing at around 838cm^{-1} may be due to the localized short-range disorder of B site atoms and subsequent relaxation of the selection rules.

Fig. 4

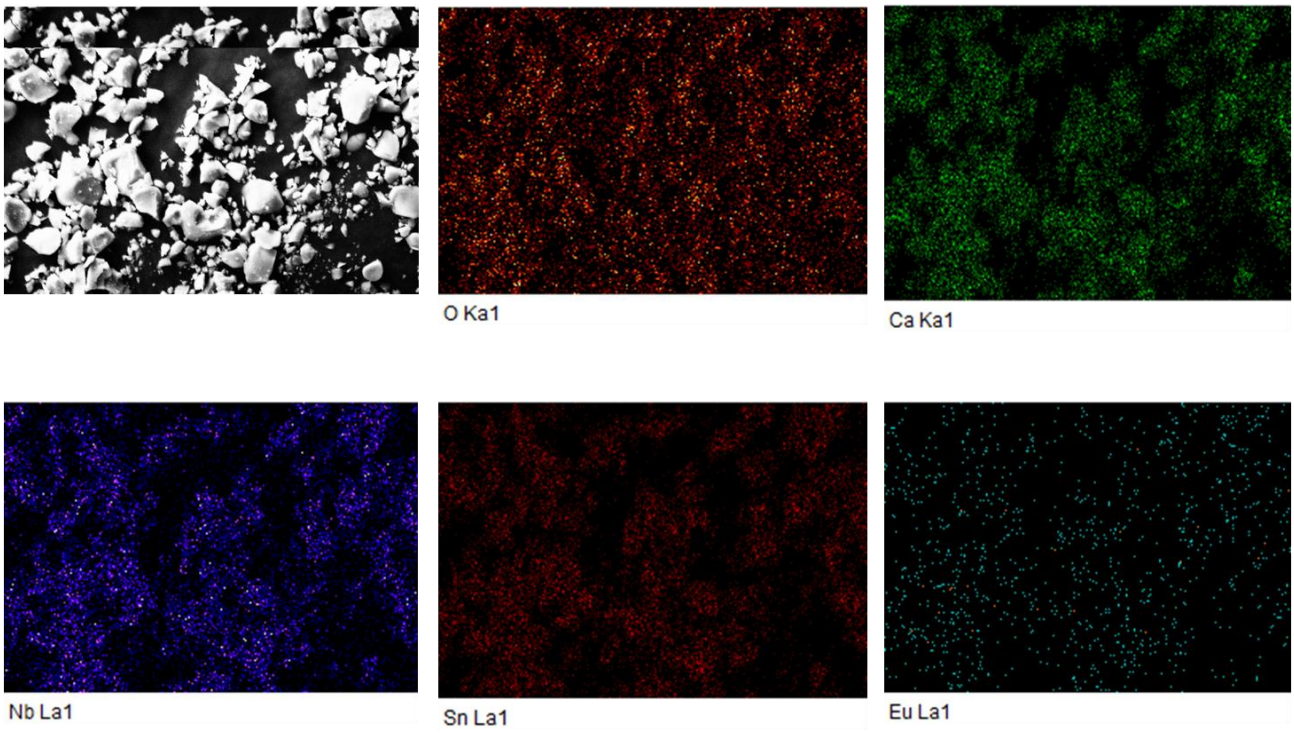

Fig. 4 Elemental X-ray dot mapping of typical $Ca_{2.85}Sn_3Nb_2O_{14}$:*0.15*Eu^{3+} phosphor synthesized at 1500°C. It confirms that all the elements are uniformly distributed in the lattice.

Fig. 5

(a) (b)

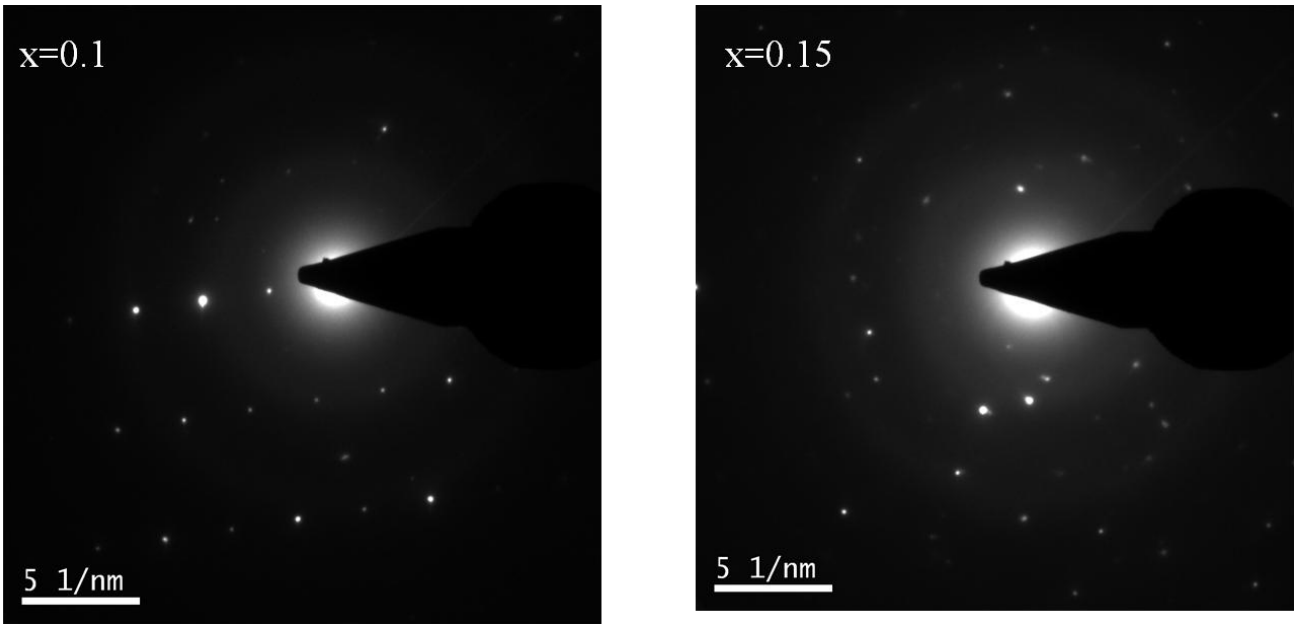

Fig. 5 Selected Area Electron Difftraction (SAED) patterns of (a) $Ca_{2.9}Sn_3Nb_2O_{14}$:*0.10*Eu^{3+} and (b) $Ca_{2.85}Sn_3Nb_2O_{14}$:*0.15*Eu^{3+} phosphors.

Fig. 6

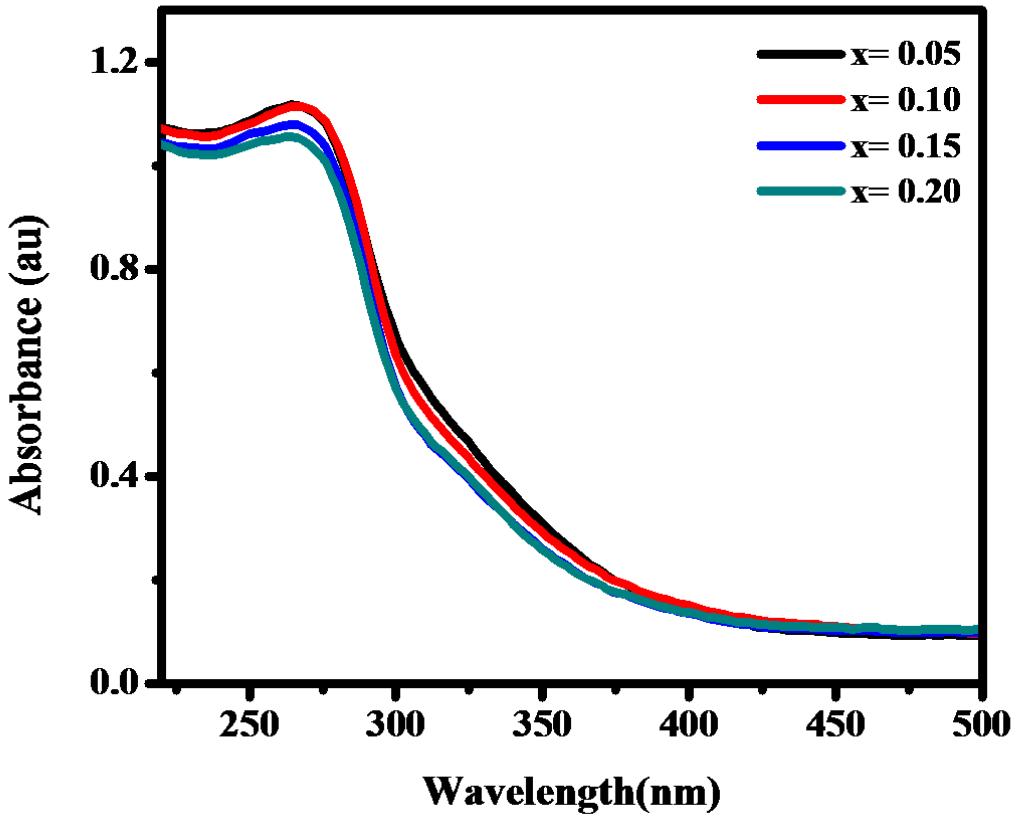

Fig. 6 UV-visible absorption spectra of $Ca_{3-x}Sn_3Nb_2O_{14}$:xEu^{3+} (x=0.05, 0.10, 0.15 and 0.20) red phosphors. The spectra showed a blue shift with increasing concentration of Eu^{3+}.

Fig. 7

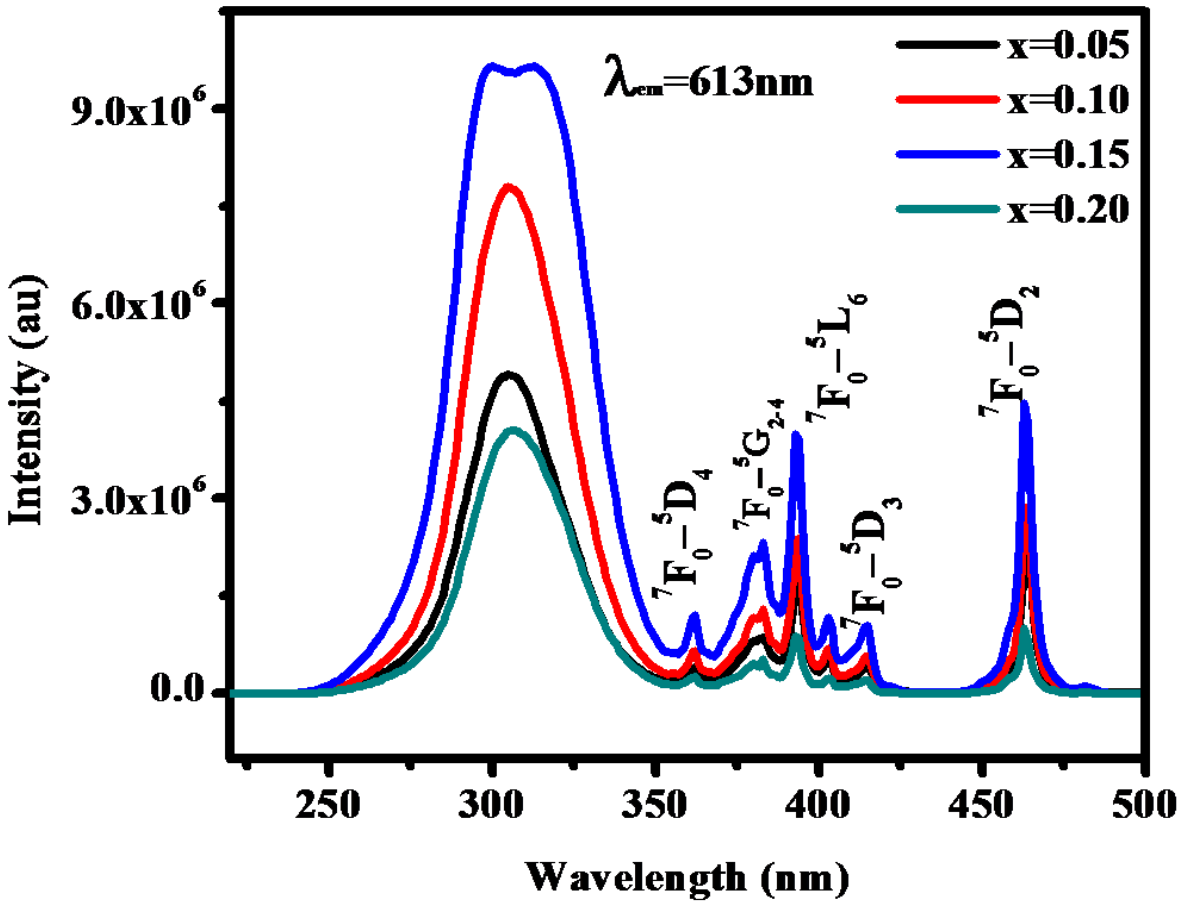

Fig. 7 Excitation spectra of $Ca_{3-x}Sn_3Nb_2O_{14}$:xEu^{3+} (x = 0.05, 0.10, 0.15, 0.20) for an emission at 613nm. The broad band from 250-360nm centered at 306nm correspond to metal-oxygen charge transfer. The sharp peaks beyond 360nm arise from the intraconfigurational f-f transitions of Eu^{3+} which are less intense compared to the broad charge transfer band and are saturated for 15mol% doping.

Fig. 8

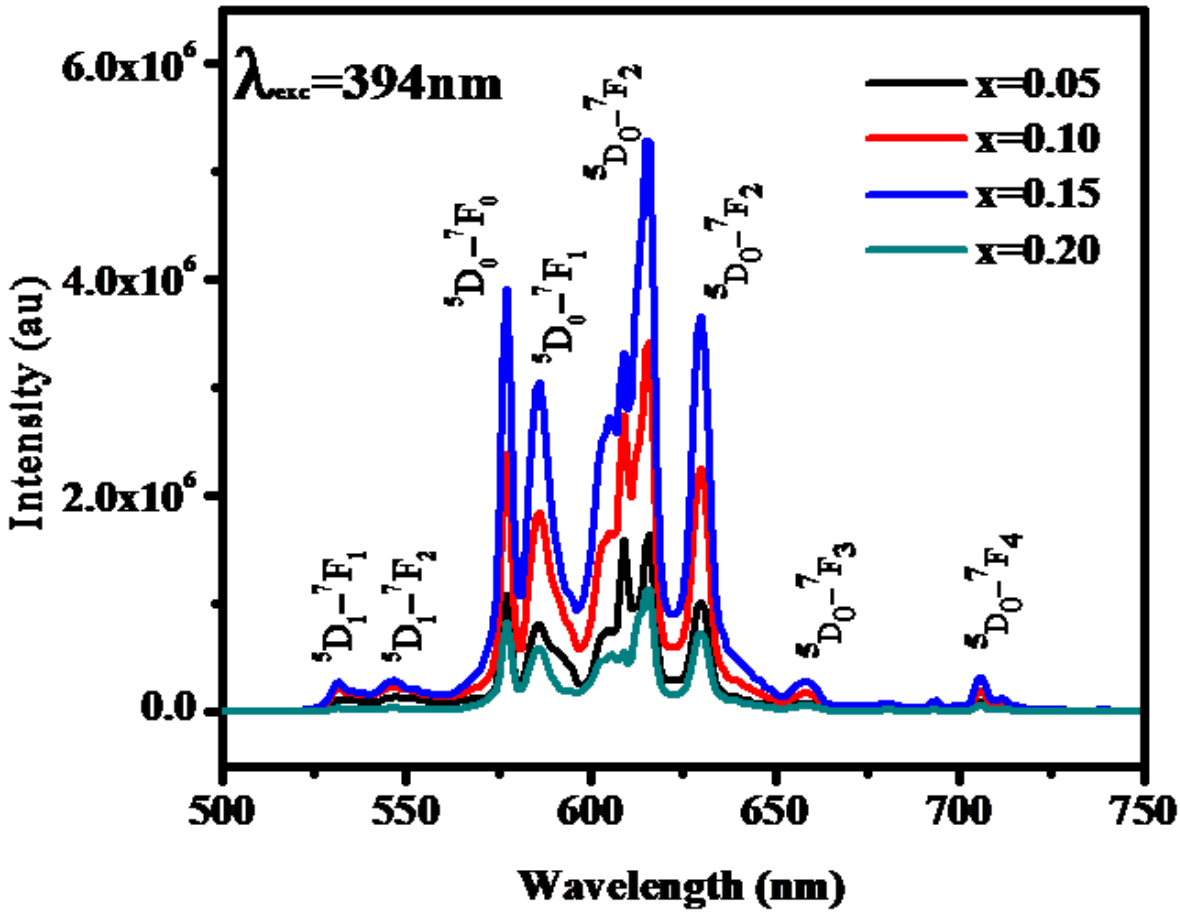

Fig. 8 The emission spectra of $Ca_{3-x}Sn_3Nb_2O_{14}$:xEu^{3+} (x = 0.05, 0.10, 0.15, and 0.20) excited at 394nm. The forbidden $^5D_0$-$^7F_0$ transition dominates over the allowed $^5D_0$-$^7F_1$ MD transition. After 15mol% doping, concentration quenching occurs.

Fig. 9

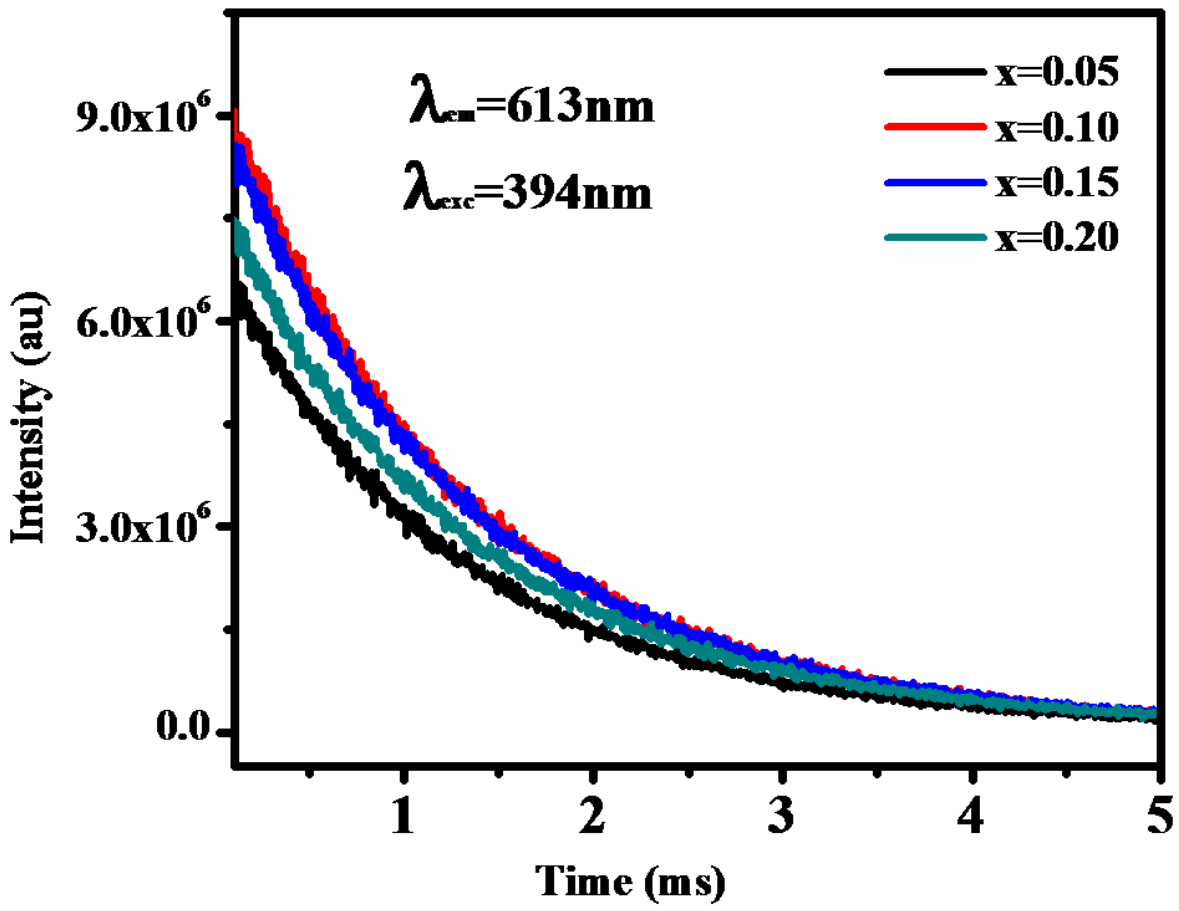

Fig. 9 Life time decay curves of $^5D_0$-$^7F_2$ transition of Eu^{3+} (wavelength 613nm) in $Ca_{3-x}Sn_3Nb_2O_{14}$:xEu^{3+} (x = 0.05, 0.10, 0.15 and 0.20) under 394nm excitation. The curves can be well fitted with a single exponential function I = Aexp(-t/τ) where I, τ, and A are intensity, decay time and fitting parameter respectively.